

UC San Diego

UC San Diego Previously Published Works

Title

Evaluating Metal-Ligand Interactions of Metal-Binding Isosteres Using Model Complexes

Permalink

<https://escholarship.org/uc/item/1q04h0s2>

Journal

Inorganic Chemistry, 60(22)

ISSN

0020-1669

Authors

Seo, Hyeonlim
Prosser, Kathleen E
Kalaj, Mark
[et al.](#)

Publication Date

2021-11-15

DOI

10.1021/acs.inorgchem.1c02433

Peer reviewed



HHS Public Access

Author manuscript

Inorg Chem. Author manuscript; available in PMC 2022 November 15.

Published in final edited form as:

Inorg Chem. 2021 November 15; 60(22): 17161–17172. doi:10.1021/acs.inorgchem.1c02433.

Evaluating Metal-ligand Interactions of Metal-binding Isosteres Using Model Complexes

Hyeonlim Seo, Kathleen E. Prosser, Mark Kalaj, Johannes Karges, Benjamin Dick, Seth M. Cohen*

Department of Chemistry and Biochemistry, University of California, San Diego, La Jolla, California, 92093, USA

Abstract

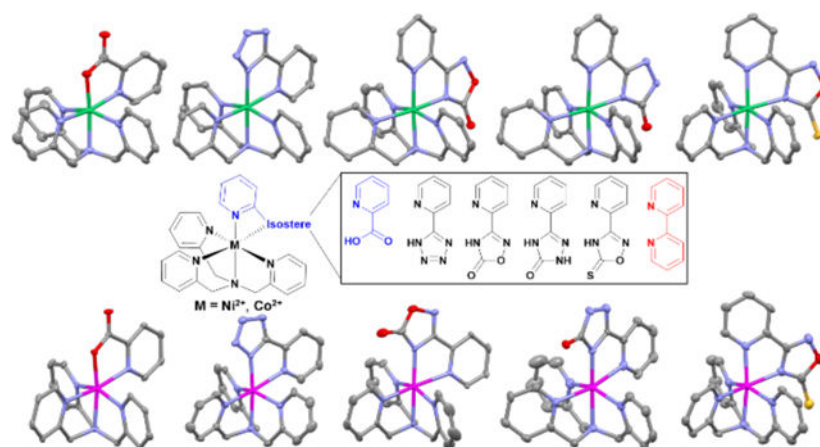
Bioisosteres are a useful approach to address pharmacokinetic liabilities and improve drug-like properties. Specific to developing metalloenzyme inhibitors, metal-binding pharmacophores (MBPs) have been combined with bioisosteres, to produce metal-binding isosteres (MBIs) as alternative scaffolds used in fragment-based drug discovery (FBDD). Picolinic acid MBIs have been reported and evaluated for their metal-binding ability, pharmacokinetic properties, and enzyme inhibitory activity. However, their structural, electronic, and spectroscopic properties with metal ions other than Zn(II) have not been reported, which might reveal similarities and differences between MBIs and the parent MBPs. To this end, $[M(\text{TPA})(\text{MBI})]$ ($M = \text{Ni}(\text{II})$ and $\text{Co}(\text{II})$, TPA = tris(2-pyridylmethyl)amine) is presented as a bioinorganic model system for investigating picolinic acid, four heterocyclic MBIs, and 2,2'-bipyridine. These complexes were characterized by X-ray crystallography, NMR, IR, and UV-vis spectroscopy, and their magnetic moments were accessed. In addition, $[(\text{Tp}^{\text{Ph,Me}})\text{Co}(\text{MBI})]$ ($\text{Tp}^{\text{Ph,Me}} = \text{hydrotris}(3,5\text{-phenylmethylpyrazolyl})\text{borate}$) was used as a second model compound and the limitations and attributes of the two model systems are discussed. These results demonstrate that bioinorganic model complexes are versatile tools for metalloenzyme inhibitor design and can provide insights into the broader use of MBIs.

Graphical Abstract

*Corresponding Author: scohen@ucsd.edu (S.M.C.).

Accession Codes. CCDC 2081976–2081900 and 2085664 contain the supplementary crystallographic data for this paper. These data can be obtained free of charge via www.ccdc.cam.ac.uk/data_request/cif, by emailing data_request@ccdc.cam.ac.uk, or by contacting The Cambridge Crystallographic Data Centre, 12 Union Road, Cambridge CB2 1EZ, UK; fax: +44 1223 336033.

The authors declare the following competing financial interest(s): S.M.C. is a co-founder, has an equity interest, and receives income as member of the Scientific Advisory Board for Forge Therapeutics; is a co-founder, has an equity interest, and is a member of the Scientific Advisory Board for Blacksmith Medicines; and is a co-founder and has an equity interest in Cleave Therapeutics (formerly Cleave Biosciences). These companies may potentially benefit from the research results of certain projects in the laboratory of S.M.C. The terms of this arrangement have been reviewed and approved by the University of California, San Diego in accordance with its conflict of interest policies.



Keywords

metalloenzyme inhibitor; fragment-based drug discovery; metal binding isosteres; isosteres

INTRODUCTION

Metalloenzymes make up approximately 40% of all enzymes.¹ Their ubiquity makes metalloenzymes important targets for therapeutics. Despite their prevalence, fewer than 5% of small molecule drugs target a metalloenzyme.¹ A barrier for developing metalloenzyme inhibitors has been the longstanding reliance on a limited number of metal-binding pharmacophores (MBPs) to bind to the active site metal ion(s) in these targets. The hydroxamic acid functional group is an archetypal MBP and it has been extensively employed to inhibit a wide range of metalloenzymes.² Issues surrounding hydroxamic acids and other commonplace MBPs include pharmacokinetic concerns such as metabolic instability and poor membrane permeability, as well as limited chemical diversity and target selectivity.²

To expand the available chemical space for targeting metalloenzymes, a diversified MBP library can be utilized for fragment-based drug discovery (FBDD).³ A previously reported MBP library, consisting of ~300 low molecular weight fragments, has been used to generate active and selective hits against a variety of metalloenzyme targets.¹ This library has been gradually expanded to include a wider range of MBPs,¹ and recently metal-binding isosteres (MBIs) have been added as a new strategy to further address the pharmacokinetic liabilities of MBPs.⁴ MBIs combine the metal-binding features of MBPs with the principles of isosteres/bioisosteres to produce ligands with even greater chemical diversity and potentially improved biological and drug-like properties. Two prior studies have examined MBIs derived from the picolinic acid MBP, examining carboxylic acid isosteres⁴ and pyridine ring isosteres of this picolinic acid.⁵ These studies demonstrated the metal-binding ability of MBIs and showed that MBIs can have a pronounced influence on physicochemical properties of these ligands while retaining inhibitory activity against metalloenzymes. These prior results indicate that isosteric replacement combined with metal-binding functional

groups can be a valuable approach to improving the drug-likeness of metalloenzyme small molecule inhibitors.

Bioinorganic model complexes have been used to validate the metal-binding properties of MBPs and MBIs.^{4, 6} Model complexes provide a facile strategy to elucidate detailed metal-ligand interactions at an atomic level that can be labor intensive to achieve using more advanced biophysical methods, such as protein crystallography or nuclear magnetic resonance (NMR) spectroscopy. Therefore, model complexes are advantageous in the early stages of metalloenzyme inhibitor development to elucidate the metal-binding capability of different MBPs/MBIs.⁴ Furthermore, they provide synthetic accessibility and flexibility that enables sophisticated structural modifications to mimic the target enzyme.^{7, 8} For example, [(Tp^{Ph,Me})Zn(L)] (Tp^{Ph,Me} = hydrotris(5,3-methylphenylpyrazolyl)borate, L = metal-binding ligand) and its derivatives have been used to model the active sites of several metalloproteins including carbonic anhydrase,⁹ liver alcohol dehydrogenases,¹⁰ and matrix metalloproteinases (Figure 1).^{11, 12} Despite the broad use of the [(Tp^{Ph,Me})Zn(L)] model system, few studies have looked at other spectator ligands (i.e., ligands other than Tp^{Ph,Me}) or metal ions beyond Zn(II) to examine MBP or MBI binding and characteristics.¹³ Alternative bioinorganic model complexes could prove helpful to understand both the structural and electronic features of MBIs.

Herein, the model complex, [M(TPA)(MBI)] (M = Ni²⁺ and Co²⁺, TPA = tris(2-pyridylmethyl)amine) has been employed to investigate the coordination chemistry and spectroscopic characteristics of MBIs (Figure 1). TPA has been used as a tetradentate ligand for biologically relevant first-row transition metal ions, while providing flexible structural modification via the pyridine moieties.^{14–23} TPA complexes of Ni(II) have been used to study Ni(II)-dependent metalloenzymes such as acireductone dioxygenase,²³ urease,²⁰ and glyoxalase I.²² In the present study, Ni(II) and Co(II) complexes were used to enable structural and spectroscopic study of MBI-metal interactions. Picolinic acid (pic), several picolinic acid MBIs, and 2,2'-bipyridine (bpy) were examined (Figure 1). Bpy was included as an additional comparative ligand because it can also be regarded as an isostere of the heterocyclic MBIs studied here. The [M(TPA)(MBI)] complexes were prepared, and their reactivity, structural features, and spectroscopic properties were investigated by X-ray crystallography, NMR, IR, UV-Vis, and magnetic moment analysis. In addition, [(Tp^{Ph,Me})Co(MBI)] complexes were similarly investigated as spectroscopically active analogues of the previously reported [(Tp^{Ph,Me})Zn(MBI)] complexes.

EXPERIMENTAL METHODS

General Experimental Details.

All reagents and solvents were obtained from commercial sources (Sigma Aldrich, Alfa Aesar, TCI, Combi-Blocks etc.) and used without further purification. Tris((2-pyridylmethyl)amine) (TPA) was synthesized using a modified literature procedure.²⁴ [(Tp^{Ph,Me})K] (Tp^{Ph,Me} = hydrotris(5,3-methylphenylpyrazolyl)borate) was prepared as previously reported.⁶ Picolinic acid and 2,2'-bipyridine were purchased from commercial suppliers. MBIs **1**, **2**, **3**, and **4** have been previously reported and were prepared according to literature procedures.⁴ [Ni(TPA)(OAc)(H₂O)]PF₆ and [Co(TPA)(OAc)]BPh₄ were prepared

using a modified literature procedure.^{19, 24} To obtain an X-ray structure of [Co(TPA)(pic)]⁺, it was necessary to use an alternative counterion, ClO₄⁻, because of its higher crystal quality and non-hygroscopic nature. [(Tp^{Ph,Me})ZnOH] and [(Tp^{Ph,Me})CoCl] was prepared according to literature methods,²⁵ and [(Tp^{Ph,Me})Co(MBI)] and [(Tp^{Ph,Me})Zn(bpy)] were prepared by a modification of the literature procedure.^{4, 13} Column chromatography was performed using a CombiFlash Rf automated system from Teledyne Isco using prepacked silica cartridges. All the solution-state characterization was carried out in DMSO to prevent any solubility issues. ¹H NMR spectra were recorded at ambient temperature on 300 MHz Bruker instrument and ¹³C NMR spectra were collected using 500 MHz Varian NMR instrument. Magnetic measurements were performed by solution ¹H NMR using the Evans' method²⁶ on a 300 MHz Bruker NMR spectrometer for all complexes performed at room temperature in an open-air system. The measurements were performed in a standard 5 mm NMR tube containing the paramagnetic sample of 20 mM dissolved in 400 – 500 μL of DMSO-*d*₆ against a co-axial reference tube filled with the same solvent. Processing of the NMR data was performed using the MestReNova 14.2 program. UV-visible spectra were recorded with the samples of 5 mM dissolved in DMSO using a Perkin-Elmer Lambda 25 spectrophotometer. Absorbance maxima are given as λ_{max} (nm) with extinction coefficients reported (ε, M⁻¹ cm⁻¹). Infrared spectra were collected on a Bruker Alpha FT-IR instrument. Mass spectra were obtained at the Molecular Mass Spectrometry Facility (MMSF) in the Department of Chemistry and Biochemistry at the University of California, San Diego.

Synthesis and Characterization of Compounds.

2-(1*H*-tetrazol-5-yl)pyridine (1).—The compound was made following a previously reported procedure.⁴ Picolinonitrile (2.00 g, 19.2 mmol) was dissolved in 20 mL of DMF. Sodium azide (1.87 g, 28.8 mmol) and ammonium chloride (1.54 g, 28.8 mmol) were added to the DMF solution and the mixture was stirred under nitrogen at 110 °C for 3 h. The reaction mixture was concentrated down almost to dryness on a rotary evaporator. Water was added to the residue and the solution was acidified to pH 2.0 using 6 M HCl. The product precipitated as a solid and was collected by filtration. The collected white solid was washed with water and dried. Yield: 2.0 g (13.6 mmol, 71%). ¹H NMR (300 MHz, DMSO-*d*₆): δ 8.81 (ddd, *J*₁ = 4.8, *J*₂ = 1.7, *J*₃ = 0.9 Hz, 1H), 8.24 (dt, *J*₁ = 7.9, *J*₂ = 1.1 Hz, 1H), 8.09 (td, *J*₁ = 7.7, *J*₂ = 1.7 Hz, 1H), 7.64 (ddd, *J*₁ = 7.6, *J*₂ = 4.8, *J*₃ = 1.2 Hz, 1H). ESI-MS (*m/z*): [M+H]⁺ calcd. for C₆H₆N₅, 148.06; found, 148.11. ATR-FTIR (neat, cm⁻¹): 1606, 1620, 1637.

3-(pyridin-2-yl)-1,2,4-oxadiazol-5(4*H*)-one (2).—The compound was made following a previously reported procedure.²⁷ *N*-Hydroxypicolinimidamide (1.37 g, 10.0 mmol) was dissolved in 20 mL of dry pyridine. Ethyl chloroformate was added to the pyridine solution and the mixture was stirred under nitrogen for 6 h at reflux. The reaction mixture was concentrated and diluted with water and a precipitate formed. The precipitate was washed with water and recrystallized from water producing beige needles, which were collected by filtration. Yield: 0.89 g (5.5 mmol, 55%). ¹H NMR (300 MHz, DMSO-*d*₆): δ 13.16 (s, 1H), 8.77 (ddd, *J*₁ = 4.8, *J*₂ = 1.6, *J*₃ = 1.0 Hz, 1H), 8.09 – 8.02 (m, 1H), 8.00 (dt, *J*₁ = 7.9, *J*₂ = 1.4

Hz, 1H), 7.67 (ddd, $J_1 = 7.3$, $J_2 = 4.8$, $J_3 = 1.5$ Hz, 1H). ESI-MS (m/z): $[M+H]^+$ calcd. for $C_7H_6N_3O_2$, 164.05; found, 164.12. ATR-FTIR (neat, cm^{-1}): 1565, 1582, 1779.

5-(pyridin-2-yl)-2,4-dihydro-3H-1,2,4-triazol-3-one (3).—The compound was made following a previously reported procedure.²⁸ Methyl picolinimidate (0.80 g, 5.9 mmol) and ethyl carbazate (0.61 g, 5.9 mmol) were melted together at 200 °C and stirred for 10 min. The resulting solid was recrystallized from EtOH to yield a white solid. Yield: 0.36 g (2.2 mmol, 37%). ¹H NMR (300 MHz, DMSO- d_6): δ 12.07 (s, 1H), 11.81 (s, 1H), 8.63 (dt, $J_1 = 4.9$, $J_2 = 1.3$ Hz, 1H), 7.93 (t, $J_1 = 1.5$ Hz, 1H), 7.92 (d, $J_1 = 1.3$ Hz, 1H), 7.52 – 7.42 (m, 1H). ESI-MS (m/z): $[M+H]^+$ calcd. for $C_7H_7N_4O$, 163.06; found, 163.22. ATR-FTIR (neat, cm^{-1}): 1600, 1713.

3-(pyridin-2-yl)-1,2,4-oxadiazole-5(4H)-thione (4).—The compound was made following a previously reported procedure.⁴ *N*-Hydroxypicolinimidamide (1.0 g, 7.3 mmol) was dissolved in 60 mL of acetonitrile. 1,1'-Thiocarbonyldiimidazole (1.94 g, 10.9 mmol) and 1,8-diazabicyclo[5.4.0]undec-7-ene (4.4 mL, 29 mmol) were added to the acetonitrile solution and the mixture was stirred under nitrogen at room temperature overnight. The reaction mixture was diluted with water and acidified with 6 M HCl until a yellow precipitate formed. The precipitate was collected by filtration, washed with water, and dried resulting in a yellow solid. Yield: 0.93 g (5.2 mmol, 71%). ¹H NMR (300 MHz, DMSO- d_6): δ 8.80 (d, $J_1 = 4.7$ Hz, 1H), 8.13 – 8.02 (m, 2H), 7.70 (ddd, $J_1 = 6.8$, $J_2 = 4.8$, $J_3 = 2.1$ Hz, 1H). ESI-MS (m/z): $[M+H]^+$ calcd. for $C_7H_6N_3OS$, 180.02; found, 180.11. ATR-FTIR (neat, cm^{-1}): 1565, 1589.

(tris(2-pyridylmethyl)amine) (TPA).—TPA was synthesized using a modified literature procedure.²⁴ In a 100 ml round bottom flask 2-(bromomethyl)pyridine hydrobromide (0.6 g, 2 mmol) and potassium carbonate (0.8 g, 6 mmol) were added to acetonitrile (30 mL), bis(pyridin-2-ylmethyl)amine (0.4 g, 0.4 mL, 2 mmol) was then added and the reaction was stirred overnight at room temperature. The reaction mixture was then filtered, and the filtrate was dried down and loaded onto silica. The product was purified via column chromatography using a CH_2Cl_2 : MeOH gradient of 0–10% ($R_f = 0.30$, 7% MeOH in CH_2Cl_2). The fraction containing the product was dried down yielding a light brown to white solid. Yield: 0.31 g (2 mmol, 50%). ¹H NMR (300 MHz, DMSO- d_6): δ 8.49 (d, $J_1 = 4.4$ Hz, 1H), 7.77 (td, $J_1 = 7.7$, $J_2 = 1.9$ Hz, 1H), 7.59 (d, $J_1 = 7.8$ Hz, 1H), 7.25 (ddd, $J_1 = 7.5$, $J_2 = 4.8$, $J_3 = 1.2$ Hz, 1H), 3.77 (s, 2H). ESI-MS (m/z): $[M+H]^+$ calcd. for $C_{18}H_{18}N_4$, 291.15; found, 291.26. ATR-FTIR (neat, cm^{-1}): 1588, 1568, 1473, 1436, 1366, 1311.

[Ni(TPA)(pic)]PF₆.—Nickel(II) acetate tetrahydrate (85.7 mg, 344 μ mol) and TPA (100 mg, 344 μ mol) were dissolved in MeOH (5 mL) and stirred for 10 min at room temperature. Picolinic acid (42 mg, 344 μ mol) was then added to the reaction vessel and stirred for another 10 min. Sodium hexafluorophosphate(V) (58 mg, 344 μ mol) was then added and stirred overnight at room temperature. A light purple solid precipitate resulted, which was collected by filtration. The resulting solid was washed with MeOH and dried. Vapor diffusion of Et₂O into a CH₃CN solution of the complex gave crystals suitable for X-ray diffraction. Yield: 39%. ATR-FTIR (neat, cm^{-1}): 557, 834 (PF₆⁻), 1603, 1018, 1051, 1646,

1363. UV-vis: 531(21). ESI-MS (m/z): $[\text{M-PF}_6]^+$ calcd. for $\text{C}_{24}\text{H}_{22}\text{N}_5\text{NiO}_2$, 470.11; found, 470.17. HR-MS (m/z): $[\text{M-PF}_6]^+$ calcd. for $\text{C}_{24}\text{H}_{22}\text{N}_5\text{NiO}_2$, 470.1121; found, 470.1125.

[Ni(TPA)(1)]PF₆.—The same procedure was used as in the synthesis of $[\text{Ni}(\text{TPA})(\text{pic})]\text{PF}_6$. The product was isolated as a purple solid. Vapor diffusion of Et_2O into a CH_3CN solution of the complex gave purple crystals suitable for X-ray diffraction. Yield: 38%. ATR-FTIR (neat, cm^{-1}): 557, 833 (PF_6^-), 1608, 1020, 1054. UV-vis: 534 (23). ESI-MS (m/z): $[\text{M-PF}_6]^+$ calcd. for $\text{C}_{24}\text{H}_{22}\text{N}_9\text{Ni}$, 494.14; found, 494.14. HR-MS (m/z): $[\text{M-PF}_6]^+$ calcd. for $\text{C}_{24}\text{H}_{22}\text{N}_9\text{Ni}$, 494.1346; found, 494.1343.

[Ni(TPA)(2)]PF₆.—The same procedure was used as in the synthesis of $[\text{Ni}(\text{TPA})(\text{pic})]\text{PF}_6$. The product was isolated as a purple solid. Vapor diffusion of Et_2O into a CH_3CN solution of the complex gave purple crystals suitable for X-ray diffraction. Yield: 37%. ATR-FTIR (neat, cm^{-1}): 557, 833 (PF_6^-), 1608, 1020, 1051, 1696, 1398. UV-vis: 548 (21). ESI-MS (m/z): $[\text{M-PF}_6]^+$ calcd. for $\text{C}_{25}\text{H}_{22}\text{N}_7\text{NiO}_2$, 510.12; found, 510.14. HR-MS (m/z): $[\text{M-PF}_6]^+$ calcd. for $\text{C}_{25}\text{H}_{22}\text{N}_7\text{NiO}_2$, 510.1183; found, 510.1181.

[Ni(TPA)(3)]PF₆.—Nickel(II) acetate tetrahydrate (86 mg, 344 μmol) and TPA (100 mg, 344 μmol) were dissolved in $i\text{PrOH}$ (5 mL) and stirred for 10 min at room temperature. 5-(Pyridin-2-yl)-2,4-dihydro-3H-1,2,4-triazol-3-one (**3**, 56 mg, 344 μmol) was then added to the reaction vessel and stirred for another 10 min. Tetrabutylammonium hexafluorophosphate(V) (133 mg, 344 μmol) was then added and stirred overnight. A light purple solid precipitate resulted, which was collected by filtration. The resulting solid was washed with $i\text{PrOH}$ and dried. Vapor diffusion of Et_2O into a CH_3CN solution of the complex gave purple crystals suitable for X-ray diffraction. Yield: 41%. ATR-FTIR (neat, cm^{-1}): 557, 834 (PF_6^-), 1606, 1023, 1052, 1625. UV-vis: 552 (19). ESI-MS (m/z): $[\text{M-PF}_6]^+$ calcd. for $\text{C}_{25}\text{H}_{23}\text{N}_8\text{NiO}$, 509.14; found, 509.14. HR-MS (m/z): $[\text{M-PF}_6]^+$ calcd. for $\text{C}_{25}\text{H}_{23}\text{N}_8\text{NiO}$, 509.1343; found, 509.1345.

[Ni(TPA)(4)]PF₆.—The same procedure was used as in the synthesis of $[\text{Ni}(\text{TPA})(\text{pic})]\text{PF}_6$. The product was a purple solid. Vapor diffusion of Et_2O into a CH_3CN solution of the complex gave purple crystals suitable for X-ray diffraction. Yield: 54%. ATR-FTIR (neat, cm^{-1}): 557, 834 (PF_6^-), 1607, 1021, 1054, 1344. UV-vis: 555 (16). ESI-MS (m/z): $[\text{M-PF}_6]^+$ calcd. for $\text{C}_{25}\text{H}_{22}\text{N}_7\text{NiOS}$, 526.10; found, 526.14. HR-MS (m/z): $[\text{M-PF}_6]^+$ calcd. for $\text{C}_{25}\text{H}_{22}\text{N}_7\text{NiOS}$, 526.0955; found, 526.0950.

[Ni(TPA)(bpy)](PF₆)₂.—To a solution of $[\text{Ni}(\text{TPA})(\text{OAc})(\text{H}_2\text{O})]\text{PF}_6$ (100 mg, 175 μmol) dissolved in MeOH (5 mL) was added 2,2'-bipyridine (27 mg, 175 μmol) and NaPF_6 (35 mg, 210 μmol). The reaction was stirred under ice bath for 2 h. The purple precipitates were collected by filtration and dried. Vapor diffusion of Et_2O into a CH_3CN solution of the complex gave purple crystals suitable for X-ray diffraction. Yield: 22%. ATR-FTIR (neat, cm^{-1}): 557, 827 (BPh_4^-), 1607, 1021, 1054. UV-vis: 557 (12). ESI-MS (m/z): $[\text{M-PF}_6]^{2+}$ calcd. for $\text{C}_{28}\text{H}_{26}\text{N}_6\text{Ni}$, 252.08; found, 252.16.

[Co(TPA)(pic)]PF₆.—Cobalt(II) acetate tetrahydrate (85.8 mg, 344 μmol) was dissolved in a mixture of MeOH (3 mL) and $i\text{PrOH}$ (2 mL). TPA (100 mg, 344 μmol) was

then dissolved to the solution, sonicated and stirred for 10 min until all pink cobalt solution was transformed into a bright green color. Picolinic acid (42 mg, 344 μmol) was added to the solution and stirred for 10 min giving brown color. Tetrabutylammonium hexafluorophosphate(V) (133 mg, 344 μmol) was added and stirred overnight. The pink precipitates were washed with a mixture of *i*PrOH and Ether. Vapor diffusion of Et_2O into a CH_3CN solution of the complex gave pink crystals suitable for X-ray diffraction. Yield: 70%. ATR-FTIR: 557, 834 (PF_6^-), 1646, 1603, 1024, 1059. UV-vis: 493 (103). ESI-MS (m/z): $[\text{M-PF}_6]^+$ calcd. for $\text{C}_{24}\text{H}_{22}\text{CoN}_5\text{O}_2$, 471.11; found, 471.11. HR-MS (m/z): $[\text{M-PF}_6]^+$ calcd. for $\text{C}_{24}\text{H}_{22}\text{CoN}_5\text{O}_2$, 471.1100; found, 471.1089.

[Co(TPA)(1)]PF₆.—The same procedure was used as in the synthesis of [Co(TPA)(pic)]PF₆. The product was a pink solid. Vapor diffusion of Et_2O into a CH_3CN solution of the complex gave pink crystals suitable for X-ray diffraction. Yield: 59%. ATR-FTIR (neat, cm^{-1}): 557, 833 (PF_6^-), 1606, 1020, 1052. UV-vis: 485 (117). ESI-MS (m/z): $[\text{M-PF}_6]^+$ calcd. for $\text{C}_{24}\text{H}_{22}\text{CoN}_9$, 495.13; found, 495.09. HR-MS (m/z): $[\text{M-PF}_6]^+$ calcd. for $\text{C}_{24}\text{H}_{22}\text{CoN}_9$, 495.1325; found, 495.1328.

[Co(TPA)(2)]PF₆.—The same procedure was used as in the synthesis of [Co(TPA)(pic)]PF₆. The product was a pink solid. Vapor diffusion of Et_2O into a CH_3CN solution of the complex gave pink crystals suitable for X-ray diffraction. Yield: 61%. ATR-FTIR (neat, cm^{-1}): 557, 833 (PF_6^-), 1606, 1023, 1052, 1713, 1731, 1398. UV-vis: 486 (64). ESI-MS (m/z): $[\text{M-PF}_6]^+$ calcd. for $\text{C}_{25}\text{H}_{22}\text{CoN}_7\text{O}_2$, 511.12; found, 511.09.

[Co(TPA)(3)]BPh₄.—5-(Pyridin-2-yl)-2,4-dihydro-3*H*-1,2,4-triazol-3-one (**3**, 8.7 mg, 54 μmol) was added into THF (5 mL) of [Co(TPA)(OAc)]BPh₄ (40 mg, 54 μmol). The solution changed color from green to brown. The solution was left to stir overnight at room temperature, resulting in pink precipitates, which were collected by filtration and dried. Vapor diffusion of cyclohexane into a CH_2Cl_2 solution of the complex gave pink crystals suitable for X-ray diffraction. Yield: 51%. ATR-FTIR (neat, cm^{-1}): 704, 732 (BPh_4^-), 1602, 1021, 1058, 1633. UV-vis: 484 (88). ESI-MS (m/z): $[\text{M-PF}_6]^+$ calcd. for $\text{C}_{25}\text{H}_{23}\text{CoN}_8\text{O}$, 510.13; found, 510.19.

[Co(TPA)(4)]BPh₄.—3-(Pyridin-2-yl)-1,2,4-oxadiazole-5(4*H*)-thione (**4**, 9.7 mg, 54 μmol) was added into THF (5 mL) of [Co(TPA)(OAc)]BPh₄ (40 mg, 54 μmol). The solution changed color from green to brown. Pink crystals suitable for X-ray diffraction were grown by slow evaporation of the complex from THF. Yield: 56%. ATR-FTIR (neat, cm^{-1}): 704, 732 (BPh_4^-), 1605, 1021, 1055, 1346. UV-vis: 483 (76). ESI-MS (m/z): $[\text{M-PF}_6]^+$ calcd. for $\text{C}_{25}\text{H}_{22}\text{CoN}_7\text{OS}$, 527.09; found, 527.09.

[(Tp^{Ph,Me})Co(pic)].—To a solution of [(Tp^{Ph,Me})CoCl] (50 mg, 87 μmol) dissolved in CH_2Cl_2 (10 mL) was added 2–3 drops of triethylamine. 1 equiv of picolinic acid (11 mg, 87 μmol) dissolved in 2 mL of MeOH to this solution, resulting in a pink-colored solution. The mixture was stirred at room temperature overnight under a nitrogen atmosphere. After stirring, the solution was evaporated to dryness to give a purple solid. The resulting precipitates was purified via silica gel chromatography eluting a gradient of 0–3% MeOH in CH_2Cl_2 ($R_f = 0.23$, 5% MeOH in CH_2Cl_2). Pinkish-purple crystals suitable for X-ray

diffraction were grown from a solution of the purified precipitates in benzene diffused with pentane. Yield: 63%. ATR-FTIR (neat, cm^{-1}): 1057, 1164, 1333, 1434, 1540, 1600, 1657, 1667, 2532 (B-H). UV-vis: 452 (41), 538 (49), 561 (51). ESI-MS (m/z): $[\text{M}+\text{Na}]^+$ calcd. for $\text{C}_{36}\text{H}_{32}\text{BCoN}_7\text{O}_2$, 687.20; found, 687.28.

$[(\text{Tp}^{\text{Ph,Me}})\text{Co}(1)]$.—The same procedure was used as in the synthesis of $[(\text{Tp}^{\text{Ph,Me}})\text{Co}(\text{pic})]$. The product was a purple solid. ($R_f = 0.18$, 5% MeOH in CH_2Cl_2). Pinkish-purple crystals suitable for X-ray diffraction were grown from a solution of the purified precipitates in benzene diffused with pentane. Yield: 70%. ATR-FTIR (neat, cm^{-1}): 1061, 1169, 1341, 1434, 1538, 1613, 2537 (B-H). UV-vis: 456 (37), 540 (49), 563 (47). ESI-MS (m/z): $[\text{M}+\text{Na}]^+$ calcd. for $\text{C}_{36}\text{H}_{32}\text{BCoN}_{11}$, 711.23; found, 711.33. HR-MS (m/z): $[\text{M}+\text{H}]^+$ calcd. for $\text{C}_{36}\text{H}_{32}\text{BCoN}_{11}$, 689.2346; found, 689.2339.

$[(\text{Tp}^{\text{Ph,Me}})\text{Co}(2)]$.—The same procedure was used as in the synthesis of $[(\text{Tp}^{\text{Ph,Me}})\text{Co}(\text{pic})]$. The product was a purple solid. ($R_f = 0.30$, 5% MeOH in CH_2Cl_2). Pinkish-purple crystals suitable for X-ray diffraction were grown from a solution of the purified precipitates in benzene diffused with pentane. Yield: 89%. ATR-FTIR (neat, cm^{-1}): 1060, 1173, 1342, 1436, 1541, 1610, 1732, 1752, 2541 (B-H). UV-vis: 448 (47), 542 (44), 562 (42). ESI-MS (m/z): $[\text{M}+\text{Na}]^+$ calcd. for $\text{C}_{36}\text{H}_{30}\text{BCoN}_9\text{O}_2$, 727.21; found, 727.25.

$[(\text{Tp}^{\text{Ph,Me}})\text{Co}(\text{bpy})]\text{PF}_6$.—To a solution of $[(\text{Tp}^{\text{Ph,Me}})\text{CoCl}]$ (50 mg, 87 μmol) dissolved in 10 mL CH_2Cl_2 was added 1 equiv of 2,2'-bipyridine (14 mg, 87 μmol) dissolved in 2 mL of MeOH. The mixture was stirred for 10 min. 2,2'-bipyridine was added and stirred at room temperature overnight under a nitrogen atmosphere. After stirring, the solution was evaporated to give a brownish orange solid. Brownish-orange crystals suitable for X-ray diffraction were grown from a solution of the precipitates in benzene diffused with pentane. Yield: 83%. ATR-FTIR (neat, cm^{-1}): 1060, 1175, 1340, 1435, 1541, 1603, 2552 (B-H). UV-vis: 417 (333), 520 (76), 676 (34). ESI-MS (m/z): $[\text{M}-\text{PF}_6]^+$ calcd. for $\text{C}_{40}\text{H}_{36}\text{BCoN}_8$, 698.25; found, 698.21. HR-MS (m/z): $[\text{M}-\text{PF}_6]^+$ calcd. for $\text{C}_{40}\text{H}_{36}\text{BCoN}_8$, 698.2489; found, 698.2484.

$[(\text{Tp}^{\text{Ph,Me}})\text{Zn}(\text{bpy})]\text{ClO}_4$.— $[(\text{Tp}^{\text{Ph,Me}})\text{ZnOH}]$ (40 mg, 71 μmol) was dissolved in 15 mL of CH_2Cl_2 . 2,2'-bipyridine (11 mg, 71 μmol) and sodium perchlorate (9mg, 71 μmol) in 10 mL of MeOH was added to the solution, and the reaction mixture was stirred at room temperature overnight under a nitrogen atmosphere. The resulting solution was evaporated to give white solid. Colorless crystals suitable for X-ray diffraction were grown from a solution of the precipitates in benzene diffused with pentane. The crystals were characterized by X-ray crystallography. Yield: 80%. HR-MS (m/z): $[\text{M}-\text{ClO}_4]^+$ calcd. for $\text{C}_{40}\text{H}_{36}\text{BZnN}_8$, 703.2449; found, 703.2443. *Caution:* Perchlorate salts of metal complexes with organic ligands are potentially explosive. Only small amounts of these materials should be prepared, and they should be handled with great care.

RESULTS AND DISCUSSION

Preparation of MBIs and model complexes.

Picolinic acid (pic), 2,2'-bipyridine (bpy), and four MBIs were examined in this study (Figure 1). The four heterocyclic carboxylic acid isosteres studied were 2-(1*H*-tetrazol-5-yl)pyridine (MBI **1**), 3-(pyridin-2-yl)-1,2,4-oxadiazol-5(4*H*)-one (MBI **2**), 5-(pyridin-2-yl)-2,4-dihydro-3*H*-1,2,4-triazol-3-one (MBI **3**), and 3-(pyridin-2-yl)-1,2,4-oxadiazole-5(4*H*)-thione (MBI **4**) (Figure 1). These heterocycles have been used as carboxylic acid isosteres in drug design to modulate key parameters, such as acidity, geometry (i.e., planarity), charge distribution, and lipophilicity.²⁹ 2,2'-Bipyridine was added as an alternative isostere of these heterocycles as it shares general structure of the other ring scaffolds, but is aprotic (neutral donor). Picolinic acid and 2,2'-bipyridine were purchased from commercial sources, while the MBIs were synthesized according to published procedures.^{4, 27, 28}

Each of the [Ni(TPA)(MBI)](PF₆) complexes including [Ni(TPA)(pic)](PF₆) were synthesized in a one-pot reaction. For complexes with pic, **1**, **2**, and **4**, an equimolar solution of Ni(CH₃CO₂)₂·4H₂O, TPA, and the respective MBI was prepared in MeOH and then NaPF₆ was added to the mixture. The resulting purple precipitates were collected by filtration and washed with MeOH. To prepare [Ni(TPA)(**3**)](PF₆), the reaction was carried out in *i*PrOH to promote precipitation of the desired complex and NBu₄PF₆ was used as a counter ion source based on the solubility of the product in *i*PrOH. Different synthetic conditions were required to make [Ni(TPA)(bpy)](PF₆)₂, as under either of the aforementioned conditions bpy formed [Ni(bpy)₃]²⁺ as the major product. [Ni(TPA)(bpy)](PF₆)₂ was obtained by first isolating the intermediate, [Ni(TPA)(CH₃CO₂)(H₂O)]PF₆, followed by the addition of a MeOH solution of one equivalent of bpy and NaPF₆ with stirring in an ice bath for 2 h to generate a purple precipitate. All Ni(II) complexes were isolated as purple solids in yields between 22–54% and vapor diffusion of Et₂O into CH₃CN solutions of the complexes gave crystals suitable for X-ray diffraction.

The synthesis and crystallization of Co(II) complexes was slightly different from the Ni(II) complexes, depending on the MBIs. [Co(TPA)(pic)](PF₆), [Co(TPA)(**1**)](PF₆), and [Co(TPA)(**2**)](PF₆) were prepared in a one-pot reaction similar to the Ni(II) complexes. Equimolar amounts of Co(CH₃CO₂)₂·4H₂O, TPA, and the respective MBI were mixed in a 1:1 mixture of *i*PrOH and MeOH, and then NBu₄PF₆ was added to the solution. Pink solids were isolated in yields between 59–70% and vapor diffusion of Et₂O into CH₃CN yielded X-ray quality crystals. To make [Co(TPA)(**3**)](BPh₄) and [Co(TPA)(**4**)](BPh₄), it was necessary to first prepare an intermediate, [Co(TPA)(CH₃CO₂)]BPh₄.¹⁹ This intermediate was then combined with one equivalent of **3** or **4** in THF. [Co(TPA)(**3**)](BPh₄) was crystallized from cyclohexane diffusion into a CH₂Cl₂ solution of the complex, while [Co(II)(TPA)(**4**)](BPh₄) was directly obtained by slow evaporation from THF in yields of 56% and 51%, respectively. The use of the [Co(TPA)(CH₃CO₂)]BPh₄ intermediate allowed formation of the desired product and prevented formation of insoluble byproducts, including homoleptic complexes (i.e., [Co(MBI)₃]). Note that while the Co(II) complexes for pic and MBIs were readily synthesized, it was challenging to obtain [Co(TPA)(bpy)]²⁺ under any

circumstance. Attempts to prepare $[\text{Co}(\text{TPA})(\text{bpy})]^{2+}$ always produced $[\text{Co}(\text{bpy})_3]^{2+}$ as the major product. This result shows that the reactivity of bpy in these TPA model systems is significantly different from pic and the MBIs.

$[(\text{Tp}^{\text{Ph,Me}})\text{Co}(\text{MBI})]$ was applied as an alternative model system with two objectives. The first objective was to compare the coordination geometry of $[(\text{Tp}^{\text{Ph,Me}})\text{Co}(\text{pic})]$ and $[(\text{Tp}^{\text{Ph,Me}})\text{Co}(\text{MBI})]$ complexes to each other and with those of the corresponding $[(\text{Tp}^{\text{Ph,Me}})\text{Zn}(\text{MBI})]$ complexes.⁴ The second goal was to examine the spectroscopic properties of $[(\text{Tp}^{\text{Ph,Me}})\text{Co}(\text{MBI})]$ with those of $[(\text{Tp}^{\text{Ph,Me}})\text{Co}(\text{pic})]$ and $[(\text{Tp}^{\text{Ph,Me}})\text{Co}(\text{bpy})]^+$, the latter of which could not be prepared using the TPA model system.

$[(\text{Tp}^{\text{Ph,Me}})\text{Co}(\text{MBI})]$ complexes were prepared via a $[(\text{Tp}^{\text{Ph,Me}})\text{Co}(\text{Cl})]$ intermediate,^{13, 25} where 1 equiv. of each ligand in MeOH was added to the solution of $[(\text{Tp}^{\text{Ph,Me}})\text{Co}(\text{Cl})]$ in CH_2Cl_2 . To prepare $\text{Tp}^{\text{Ph,Me}}$ complexes coordinated with pic and its MBIs, excess triethylamine (TEA) was required to prevent acid-promoted decomposition of the $[(\text{Tp}^{\text{Ph,Me}})\text{Co}(\text{Cl})]$. NaPF_6 was added as a counterion to produce $[(\text{Tp}^{\text{Ph,Me}})\text{Co}(\text{bpy})]\text{PF}_6$. Pinkish-purple solids were isolated for $[(\text{Tp}^{\text{Ph,Me}})\text{Co}(\text{pic})]$, $[(\text{Tp}^{\text{Ph,Me}})\text{Co}(\mathbf{1})]$ and $[(\text{Tp}^{\text{Ph,Me}})\text{Co}(\mathbf{2})]$, while $[(\text{Tp}^{\text{Ph,Me}})\text{Co}(\text{bpy})]\text{PF}_6$ gave brownish-orange colored solid in good yields. The complexes were recrystallized by diffusing pentane into a solution of the complex in benzene. MBIs **3** and **4** generated $[\text{Co}(\text{pz}^{\text{Ph,Me}})_2(\text{MBI})_2]$ ($\text{pz}^{\text{Ph,Me}} = 5,3$ -methylphenylpyrazole) as a major product (confirmed by X-ray crystallography, data not shown). This result is tentatively attributed to both the intrinsic instability of the starting material, $[(\text{Tp}^{\text{Ph,Me}})\text{Co}(\text{Cl})]$,^{13, 30} and different metal-binding properties of MBI **3** and **4**, as observed in $[(\text{Tp}^{\text{Ph,Me}})\text{Zn}(\text{MBI})]$ system.⁴

Structural analysis.

$[(\text{Tp}^{\text{Ph,Me}})\text{Zn}(\text{MBI})]$ complexes of pic, **1**, **2**, **3**, and **4** have been previously reported and show bidentate binding to the Zn(II) ion in all cases.^{4, 31} In addition, the $\text{Tp}^{\text{Ph,Me}}$ spectator ligand in $[(\text{Tp}^{\text{Ph,Me}})\text{Zn}(\text{MBI})]$ complexes of pic, **1**, and **2** show the expected tridentate binding, while with **3** and **4**, an unexpected coordination mode where a water molecule displaces one of the pyrazole arms of the $\text{Tp}^{\text{Ph,Me}}$ ligand was reported.⁴ Herein, the structural features of $[\text{M}(\text{TPA})(\text{pic})]^+$, $[\text{M}(\text{TPA})(\text{MBI})]^+$ and $[\text{M}(\text{TPA})(\text{bpy})]^{2+}$ complexes were examined in the context of the previously reported $[(\text{Tp}^{\text{Ph,Me}})\text{Zn}(\text{MBI})]$ complexes.

MBIs bound to the TPA complexes showed a bidentate mode of coordination, generating metal ion centres with distorted octahedral geometries (Figures 2 and 3). The bite angles of MBI ligands (N5-M-N6) decreased compared to that of the parent pic complexes (N5-M-O1) (Tables 1 and 2). This trend was expected because of the rigidity of the heterocyclic isosteres. $[\text{M}(\text{TPA})(\mathbf{1})]^+$ showed the most significant decrease in bite angle by $\sim 2.1^\circ$ and $\sim 3.8^\circ$ for the Ni(II) and Co(II) complexes, respectively (Table 1 and 2). All MBIs showed slightly longer bond distances ($>0.1 \text{ \AA}$) compared to the parent pic complexes. For all TPA complexes, the bond lengths between the metal ions and the tertiary nitrogen donor atom of TPA were similar ($<0.1 \text{ \AA}$) (Table S5 and S6) and were consistent with previously reported values.^{23, 32–35}

Some differences in metal binding orientation between Ni(II) and Co(II) complexes were observed. Pic, **1** and **4** showed the same binding orientation regardless of the metal ion, with $[M(\text{TPA})(\text{pic})]^+$ and $[M(\text{TPA})(\mathbf{1})]^+$ positioning the pyridine ring nitrogen atom (N5) of the MBI cis to the bridgehead nitrogen (N1) of TPA while $[M(\text{TPA})(\mathbf{4})]^+$ had the N5 of the MBI trans to N1 of TPA. $[\text{Ni}(\text{TPA})(\mathbf{2})]^+$ and $[\text{Ni}(\text{TPA})(\mathbf{3})]^+$ bound such that N5 were trans to N1 of TPA while the corresponding Co(II) complexes showed the opposite (i.e., cis) orientation. The results suggest that subtle differences in metal ion coordination preferences influence how these MBIs bind to metals. Another observation is that the bite angles of the Co(II) complexes were smaller than the Ni(II) complexes (Tables 1 and 2). In addition, the Co(II) complexes are much more distorted than the Ni(II) complexes based on angular distortion parameter τ and Θ (Tables 1 and 2).^{36, 37} The higher degree of distortion observed in the Co(II) complexes can be explained by a subtle change in electronics and energetics of each complex including Jahn-Teller distortion which are commonly found in six-coordinate Co(II) complexes.^{38, 39} Overall, all MBIs showed slightly different, but not particularly notable, structural features when compared to the parent pic complex. The structure features of the $[\text{Ni}(\text{TPA})(\text{MBI})]^+$ complexes were also generally similar to those found with $[\text{Ni}(\text{TPA})(\text{bpy})]^{2+}$ (Figure 2, Table 1).

To have a better understanding of how the MBIs studied here are similar to pic or bpy, the structural features of $[(\text{Tp}^{\text{Ph,Me}})\text{Co}(\mathbf{1})]$ and $[(\text{Tp}^{\text{Ph,Me}})\text{Co}(\mathbf{2})]$ were compared with those of $[(\text{Tp}^{\text{Ph,Me}})\text{Co}(\text{pic})]$ and $[(\text{Tp}^{\text{Ph,Me}})\text{Co}(\text{bpy})]^+$ (Figure 4). In all cases, pic, **1**, **2**, and bpy showed bidentate coordination to the Co(II) center, as found for $[(\text{Tp}^{\text{Ph,Me}})\text{Zn}(\text{MBI})]$ complexes as well (Figure S1).⁴ $[(\text{Tp}^{\text{Ph,Me}})\text{Co}(\text{pic})]$ resulted in trigonal bipyramidal geometry ($\tau = 0.71$), which is isomorphous with $[(\text{Tp}^{\text{Ph,Me}})\text{Zn}(\text{pic})]$ ($\tau = 0.72$). By contrast, $[(\text{Tp}^{\text{Ph,Me}})\text{Co}(\mathbf{1})]$ and $[(\text{Tp}^{\text{Ph,Me}})\text{Co}(\mathbf{2})]$ showed distorted square pyramidal geometries ($\tau = 0.32$ and 0.41 , respectively) when compared to the analogous Zn(II) complexes ($\tau = 0.52$ and 0.55 , respectively). Bpy formed a more square pyramidal geometry with both Co(II) and Zn(II) complexes ($\tau = 0.01$ and 0.11 , respectively). This pattern of Co(II) complexes trending toward square pyramidal geometry was expected, as the trigonal bipyramidal geometry is less likely to be preferred relative to square pyramidal in 5-coordinate d^7 complexes due to ligand field stabilization energy.^{13, 40} The structural features of MBI **3** and **4** could not be compared as they could not be prepared under the same synthetic conditions used with pic, MBI **1** and **2**. Interestingly, ligands **3** and **4** showed different coordination behaviour from pic, **1**, and **2** in $[(\text{Tp}^{\text{Ph,Me}})\text{Zn}(\text{MBI})]$ system,⁴ which suggests that MBI **3** and **4** might also have different metal-binding behavior in $[(\text{Tp}^{\text{Ph,Me}})\text{Co}(\text{MBI})]$ system.

Computational analysis.

In order to understand the energetics and in particular the crystallographic findings of the MBIs in the model complexes, density functional theory (DFT) calculations for MBIs **1** - **4** in the TPA model system complexes were performed. All calculations were carried out at the wB97x-D/LanL2DZ level of theory. The computations were performed under standard conditions (1 atm, 298 K) in the gas phase to exclude any solvent or crystal packing effects which might have been observed under experimental conditions.

The bond lengths and angles of the computationally optimized structures (Table S7) were compared with the crystallographically determined ones (Tables 1 and 2). The biggest difference in bond length (0.027 Å) and bite angle (1.1°) was observed for [Ni(TPA)(**1**)]⁺. Overall, a very good agreement between the experimentally determined and theoretically calculated structures was observed with the same trends as described between the MBIs and the corresponding metals. This indicates that the calculated structures accurately reproduce the experimentally characterized complexes.

To investigate the difference in binding orientation of the N5 of MBIs either cis or trans to the N1 of TPA, the difference in energy between these isomers was calculated. The crystallographically described binding orientation of the MBIs (Figure 2 and 3) were also found to possess the lowest calculated energy, confirming that the structures correspond to the inherent preferred orientation of the MBI (Figure 5). The direct comparison between coordination orientation isomers indicates that there are energy differences of between 2.3–4.2 kcal/mol. The biggest difference in energy was observed for MBI **1** ($\Delta G = 3.6 - 4.4$ kcal/mol) and MBI **4** ($\Delta G = 3.8 - 4.2$ kcal/mol), which showed the same orientation of the MBI pyridine N5 to N1 of TPA in the corresponding Ni(II) and Co(II) complexes.

This result suggests that MBI **1** and **4** favors a specific coordination orientation independent from the central metal ion. By contrast, a somewhat smaller energy difference ($\Delta G = 2.3 - 3.1$ kcal/mol) was observed for MBI **2** and **3**, which show different binding orientations in the crystallographically characterized metal complexes. While the Ni(II) complexes of these MBIs favor a trans coordination of the N5 to the N1, a cis binding coordination preferred in the analogous Co(II) complexes. Note that the energy differences between these two different conformations is still quite small (<5.0 kcal/mol), suggesting that the binding orientation of the MBIs could be readily perturbed by the metalloenzyme active site.

Spectroscopic Analysis.

A distinct feature of both Ni(II) and Co(II) is that they are paramagnetic and have unpaired electrons – 2 for Ni(II) and either 3 or 1 for Co(II)) depending on the spin state. While the typical ¹H NMR spectra fall between 0 and 14 ppm, the ¹H resonances of Ni(II) and Co(II) complexes can often be found from –30 to 160 ppm. Paramagnetic ¹H NMR has been a useful tool for characterizing active site structural features of Co(II)-substituted Zn(II)-dependant enzymes including liver alcohol dehydrogenase⁴¹ as well as monitoring model reactions relevant to Ni(II)-containing metalloenzyme such as acireductone dioxygenase.^{23, 42} To evaluate the coordination complexes formed herein the ¹H NMR spectra of all complexes were obtained (Figures S2 and S3). The paramagnetically shifted resonances of the TPA complexes were observed, which was used for to confirm the stability and solution characteristics of the complexes. For the Ni(II) complexes, broad peaks between 30 – 70 ppm were assigned as the β-protons of TPA pyridyl rings based on ¹H NMR resonances of structurally related Ni(II) complexes (Figure S2).²³ It is interesting to note that all of the Ni(II) complexes, except [Ni(TPA)(bpy)]²⁺, showed more than two peaks in the range of 30 – 70 ppm, suggesting that the asymmetric scaffold of the MBIs in solution might cause magnetically inequivalence in the β-protons of the TPA spectator ligand. Paramagnetic ¹H NMR resonances of the Co(II) complexes showed sharper peaks

compared to the Ni(II) complexes (Figure S3). Note that the ^1H NMR resonances of $[\text{Co}(\text{TPA})(\mathbf{4})]^+$ showed a distinct spectrum, having only one sharp peak between 35 and 75 ppm while the other complexes showed more than two peaks in this same region of the spectra. Typically, in this region, β -protons of TPA pyridyl rings are found in structurally related Co(II) complexes.^{20, 42} Interestingly, $[\text{Co}(\text{TPA})(\mathbf{4})]^+$ is the only compound that showed a different binding orientation in the solid state, where the N5 was trans to the N1 of TPA (in all the other $[\text{Co}(\text{TPA})(\text{MBI})]^+$ complexes a cis orientation was observed). This suggests that **4** could have distinct binding characteristics both in solution and in the solid state when bound to Co(II) TPA complexes.

The magnetic properties of the Ni(II) and Co(II) complexes were examined to confirm the oxidation and spin state of each TPA complex. This measurement was especially meaningful for Co(II) complexes as they can adopt either high spin or low spin states while Ni(II) complexes should display two unpaired electrons in all cases.⁴³ The solution magnetic moment of all complexes were determined by the Evans method in $\text{DMSO}-d_6$ (Table 4).²⁶ The Ni(II) complexes were found to exhibit magnetic moments between $3.09 - 3.34 \mu_{\text{B}}$, which is higher than the spin-only magnetic moment for Ni(II) ($2.8 \mu_{\text{B}}$) due to spin-orbit coupling.⁴⁴ These values confirm that Ni(II) complexes have two unpaired electrons and are well within the range predicted for high spin six-coordinate Ni(II).⁴⁴ Similarly, the Co(II) complexes had magnetic moments from $4.56 - 4.76 \mu_{\text{B}}$, which are higher than the spin-only value for Co(II) ($3.9 \mu_{\text{B}}$).⁴⁴ These magnetic moments correspond to three unpaired electrons per Co(II) ion and are in good agreement with those observed for most high-spin octahedral Co(II) complexes.^{45, 46} This result is consistent with the distortion of the TPA Co(II) system observed in solid-state X-ray structural data. The ground state of an octahedral high spin d^7 complex is $^4T_{1g}$ that is Jahn-Teller active.^{39, 47}

The UV-vis spectra of the TPA complexes were also measured, and all spectra showed a strong absorption at <400 nm. For the Ni(II) TPA complexes, all compounds had a single absorption in the region $400-700$ nm, which was found in structurally related octahedral Ni(II) complexes (Table 4 and Figure S4).⁴⁸ The absorption maximum for $[\text{Ni}(\text{TPA})(\mathbf{1})](\text{PF}_6)$ (531 nm) was similar to that for $[\text{Ni}(\text{TPA})(\text{pic})](\text{PF}_6)$ (534 nm) while the other MBI complexes were clustered around 550 nm. This difference in absorption maxima is likely related to a combination of factors including the different binding orientations between MBI **1** versus **2**, **3**, and **4**. Note that the absorption maxima of $[\text{Ni}(\text{TPA})(\text{MBI})]^+$ complexes were more similar to that generated with pic than bpy in the Ni(II) systems. The UV-vis spectra of the Co(II) complexes showed one major absorption band in the range of $400 - 700$ nm consistent with previously reported high-spin octahedral Co(II) complexes (Table 4 and Figure S5).⁴⁹ All the $[\text{Co}(\text{TPA})(\text{MBI})]^+$ complexes showed a similar range of absorption wavelength maxima ($483 - 486$ nm), which was slightly shifted from the value for $[\text{Co}(\text{TPA})(\text{pic})]^+$ (493 nm).

Finally, spectroscopic characterization of the $[(\text{Tp}^{\text{Ph,Me}})\text{Co}(\text{MBI})]$ complexes was carried out to further understand the electronic difference between MBIs, pic, and bpy in the model systems. Regarding magnetic moments, pic, **1**, and **2** showed a similar range of magnetic moments around $4.84 \mu_{\text{B}}$ for each complex while bpy had a value of $4.66 \mu_{\text{B}}$. These values are in the range of those observed for other 5-coordinate, high-spin Co(II) complexes.⁴⁶ UV-

vis data showed that there are three main absorption bands in the visible range. Interestingly, [(Tp^{Ph,Me})Co(pic)], [(Tp^{Ph,Me})Co(**1**)], and [(Tp^{Ph,Me})Co(**2**)] showed similar UV-vis spectra, while the spectrum of [(Tp^{Ph,Me})Co(bpy)] was clearly different from the others (Table 5 and Figure S6). These results suggest that MBIs **1** and **2** are electronically more similar to pic than bpy in these model systems.

CONCLUSIONS

A TPA model system was used to provide structural and electronic information on picolinic acid and its MBIs. Their coordination modes were determined from X-ray crystallography and DFT calculations were used to evaluate the energetic differences in binding conformations. From these data it was determined that all four heterocyclic MBIs retain bidentate coordination to the metal centers and small energetic disparities in binding geometries can explain differences in MBI binding orientation. NMR, UV-vis, and magnetic moment analysis indicate that each MBI displays slightly different electronic characteristics while retaining overall similarities in oxidation states and spin states. In addition, the comparison of MBIs to pic and bpy indicate that these MBIs are better described as isosteres of picolinic acid than 2,2'-bipyridine. Furthermore, the investigation of [(Tp^{Ph,Me})Co(MBI)] as a secondary model complex underlines the need to use a different model systems to best implement isosteric replacement for metalloenzyme inhibition. This work demonstrates that the binding of MBIs can be influenced by several factors including structural and electronic nature of MBIs, the active site metal ion, the spectator ligand (TPA vs Tp^{Ph,Me}), and by analogy the metalloenzyme active site environment. When using model complexes other factors to be considered when translating these findings to the biological targets, such as steric constraints presented by the metalloenzyme, polar/nonpolar pockets, presence or absence of H-bond acceptors/donors, and potential competition from biological anions. Making broader use of model systems provides a better understanding of MBIs, and the results studied here will prove useful when optimizing important factors in the rational design of metalloenzyme inhibitors.

Supplementary Material

Refer to Web version on PubMed Central for supplementary material.

ACKNOWLEDGMENT

Support was provided by the National Institutes of Health (R01 AI149444) and a Natural Sciences and Engineering and Research Council of Canada Postdoctoral Fellowship (to K.E.P.). M. K. was supported by the Department of Defense (DoD) through the National Defense Science and Engineering Graduate (NDSEG) Fellowship Program is a recipient of an Achievement Rewards for College Scientists (ARCS) Foundation Fellowship. This research was supported in part by W. M. Keck Foundation through computing resources at the W. M. Keck Laboratory for Integrated Biology. We thank Dr. Milan Gembicky and Dr. Jake Bailey (U.C. San Diego) for assistance with crystallographic data collection and structure determination. We also thank Dr. Yongxuan Su for mass spectrometry analysis at the Molecular Mass Spectrometry Facility at U.C. San Diego.

REFERENCES

1. Chen AY; Adamek RN; Dick BL; Credille CV; Morrison CN; Cohen SM Targeting Metalloenzymes for Therapeutic Intervention. *Chem. Rev* 2019, 119 (2), 1323–1455. [PubMed: 30192523]

2. Cohen SM A Bioinorganic Approach to Fragment-Based Drug Discovery Targeting Metalloenzymes. *Acc. Chem. Res* 2017, 50 (8), 2007–2016. [PubMed: 28715203]
3. Erlanson DA; Fesik SW; Hubbard RE; Jahnke W; Jhoti H Twenty years on: the impact of fragments on drug discovery. *Nat. Rev. Drug Discov* 2016, 15 (9), 605–619. [PubMed: 27417849]
4. Dick BL; Cohen SM Metal-Binding Isosteres as New Scaffolds for Metalloenzyme Inhibitors. *Inorg. Chem* 2018, 57 (15), 9538–9543. [PubMed: 30009599]
5. Dick BL; Patel A; Cohen SM Effect of heterocycle content on metal binding isostere coordination. *Chem. Sci* 2020, 11 (26), 6907–6914. [PubMed: 33209243]
6. Puerta DT; Cohen SM Elucidating Drug-Metalloprotein Interactions with Tris(pyrazolyl)borate Model Complexes[†]. *Inorg. Chem* 2002, 41 (20), 5075–5082. [PubMed: 12354040]
7. Adam SM; Wijeratne GB; Rogler PJ; Diaz DE; Quist DA; Liu JJ; Karlin KD Synthetic Fe/Cu Complexes: Toward Understanding Heme-Copper Oxidase Structure and Function. *Chem. Rev* 2018, 118 (22), 10840–11022. [PubMed: 30372042]
8. Tanifuji K; Ohki Y Metal–Sulfur Compounds in N₂ Reduction and Nitrogenase-Related Chemistry. *Chem. Rev* 2020, 120 (12), 5194–5251. [PubMed: 32459087]
9. Kimblin C; Parkin G Comparison of Zinc and Cadmium Coordination Environments in Synthetic Analogues of Carbonic Anhydrase: Synthesis and Structure of {[Pim^{Pri,But}]Cd(OH₂)(OCIO₃)}(ClO₄). *Inorg. Chem* 1996, 35 (24), 6912–6913. [PubMed: 11666864]
10. Tesmer M; Shu M; Vahrenkamp H Sulfur-Rich Zinc Chemistry: New Tris(thioimidazolyl)hydroborate Ligands and Their Zinc Complex Chemistry Related to the Structure and Function of Alcohol Dehydrogenase. *Inorg. Chem* 2001, 40 (16), 4022–4029. [PubMed: 11466063]
11. Puerta DT; Cohen SM Examination of Novel Zinc-Binding Groups for Use in Matrix Metalloproteinase Inhibitors. *Inorg. Chem* 2003, 42 (11), 3423–3430. [PubMed: 12767177]
12. Puerta DT; Lewis JA; Cohen SM New Beginnings for Matrix Metalloproteinase Inhibitors: Identification of High-Affinity Zinc-Binding Groups. *J. Am. Chem. Soc* 2004, 126 (27), 8388–8389. [PubMed: 15237990]
13. Jacobsen FE; Breece RM; Myers WK; Tierney DL; Cohen SM Model Complexes of Cobalt-Substituted Matrix Metalloproteinases: Tools for Inhibitor Design. *Inorg. Chem* 2006, 45 (18), 7306–7315. [PubMed: 16933932]
14. Wang H-Y; Mijangos E; Ott S; Thapper A Water Oxidation Catalyzed by a Dinuclear Cobalt–Polypyridine Complex. *Angew. Chem. Int. Ed* 2014, 53 (52), 14499–14502.
15. Bonnitcha PD; Kim BJ; Hocking RK; Clegg JK; Turner P; Neville SM; Hambley TW Cobalt complexes with tripodal ligands: implications for the design of drug chaperones. *Dalton Trans.* 2012, 41 (37), 11293. [PubMed: 22885674]
16. Culpitt T; Guzei IA; Spencer LC; Simonson A; Miller JS; Wimmer MR; Nelson KJ Synthesis, crystal structures, and characterization of 4,5-diaza-9-[4,5-bis(methylthio)-1,3-dithiol-2-ylidene]-fluorene (L) metal complexes [(TPyA)M^{II}(L)](SbF₆)₂ (M^{II} = Mn, Fe, Co; TPyA=tris(2-pyridylmethyl)amine). *Inorg. Chim. Acta* 2015, 427, 162–167.
17. Massoud SS; Perkins RS; Louka FR; Xu W; Roux AL; Dutercq Q; Fischer RC; Mautner FA; Handa M; Hiraoka Y; Kreft GL; Bortolotto T; Terenzi H Efficient hydrolytic cleavage of plasmid DNA by chloro-cobalt(II) complexes based on sterically hindered pyridyl tripod tetraamine ligands: synthesis, crystal structure and DNA cleavage. *Dalton Trans.* 2014, 43 (26), 10086–10103. [PubMed: 24872210]
18. Melchior A; Tolazzi M Co(II) complexes with tripodal N-donor ligands: Thermodynamics of formation in anaerobic conditions and oxygen binding. *Inorg. Chim. Acta* 2011, 367 (1), 120–126.
19. Nagataki T; Tachi Y; Itoh S Ni^{II}(TPA) as an efficient catalyst for alkane hydroxylation with m-CPBA. *Chem. Commun* 2006, (38), 4016–4018.
20. Rudzka K; Arif AM; Berreau LM Chemistry of a Ni(II) Acetohydroxamic Acid Complex: Formation, Reactivity with Water, and Attempted Preparation of Zinc and Cobalt Analogues. *Inorg. Chem* 2005, 44 (20), 7234–7242. [PubMed: 16180888]
21. Chan SL-F; Lam TL; Yang C; Lai J; Cao B; Zhou Z; Zhu Q Cobalt(II) tris(2-pyridylmethyl)amine complexes [Co(TPA)X]⁺ bearing coordinating anion (X=Cl⁻, Br⁻, I⁻ and NCS⁻): synthesis and application for carbon dioxide reduction. *Polyhedron* 2017, 125, 156–163.

22. Rudzka K; Arif AM; Berreau LM Glyoxalase I-type Hemithioacetal Isomerization Reactivity of a Mononuclear Ni(II) Deprotonated Amide Complex. *J. Am. Chem. Soc* 2006, 128 (51), 17018–17023. [PubMed: 17177453]
23. Szajna E; Dobrowolski P; Fuller AL; Arif AM; Berreau LM NMR Studies of Mononuclear Octahedral Ni(II) Complexes Supported by Tris((2-pyridyl)methyl)amine-Type Ligands. *Inorg. Chem* 2004, 43 (13), 3988–3997. [PubMed: 15206880]
24. Gransbury GK; Livesay BN; Janetzki JT; Hay MA; Gable RW; Shores MP; Starikova A; Boskovic C Understanding the Origin of One- or Two-Step Valence Tautomeric Transitions in Bis(dioxolene)-Bridged Dinuclear Cobalt Complexes. *J. Am. Chem. Soc* 2020, 142 (24), 10692–10704. [PubMed: 32412246]
25. Uehara K; Hikichi S; Akita M Highly labile cationic tris-acetonitrile complexes, $[\text{Tp}^{\text{R}}\text{M}(\text{NCMe})_3]\text{OTf}$ (M = Ni, Co; Tp^{R} : hydrotrispyrazolylborato, R = Ph, Me and $i\text{Pr}_2$): versatile precursors for Tp^{R} -containing nickel and cobalt complexes. *J. Chem. Soc., Dalton Trans* 2002, (18), 3529–3538.
26. Evans DF 400. The determination of the paramagnetic susceptibility of substances in solution by nuclear magnetic resonance. *J. Chem. Soc* 1959, 2003–2005.
27. Gobis K; Foks H; K dzia A; Wierzbowska M; Zwolska Z Synthesis and antibacterial activity of novel pyridine and pyrazine derivatives obtained from amidoximes. *J. Heterocycl. Chem* 2009, 46 (6), 1271–1279.
28. Dowell RI; Hales NH; Tucker H Novel inhibitors of prolyl 4-hydroxylase. Part 4 pyridine-2-carboxylic acid analogues with alternative 2-substituents. *Eur. J. Med. Chem* 1993, 28 (6), 513–516.
29. Ballatore C; Huryn DM; Smith AB Carboxylic Acid (Bio)Isosteres in Drug Design. *ChemMedChem* 2013, 8 (3), 385–395. [PubMed: 23361977]
30. Hammes BS; Luo X; Chohan BS; Carrano MW; Carrano CJ Metal complexes of 3-carboxyethyl substituted trispyrazolylborates: interactions with the ester carbonyl oxygens. *J. Chem. Soc., Dalton Trans* 2002, (17), 3374–3380.
31. Jacobsen FE; Lewis JA; Cohen SM A New Role for Old Ligands: Discerning Chelators for Zinc Metalloproteinases. *J. Am. Chem. Soc* 2006, 128 (10), 3156–3157. [PubMed: 16522091]
32. Woods TJ; Stout HD; Dolinar BS; Vignesh KR; Ballesteros-Rivas MF; Achim C; Dunbar KR Strong Ferromagnetic Exchange Coupling Mediated by a Bridging Tetrazine Radical in a Dinuclear Nickel Complex. *Inorg. Chem* 2017, 56 (20), 12094–12097. [PubMed: 28945087]
33. van der Meer M; Rechkemmer Y; Frank U; Breitgoff FD; Hohloch S; Su C-Y; Neugebauer P; Marx R; Dörfel M; van Slageren J; Sarkar B A Dicobalt Complex with an Unsymmetrical Quinonoid Bridge Isolated in Three Units of Charge: A Combined Structural, (Spectro)electrochemical, Magnetic and Spectroscopic Study. *Chem. Eur. J* 2016, 22 (39), 13884–13893. [PubMed: 27549247]
34. Areas ES; de Assunção Paiva JL; Ribeiro FV; Pereira TM; Kummerle AE; Silva H; Guedes GP; Cellis do Nascimento AC; da Silva Miranda F; Neves AP Redox-Activated Drug Delivery Properties and Cytotoxicity of Cobalt Complexes Based on a Fluorescent Coumarin- β -Keto Ester Hybrid. *Eur. J. Inorg. Chem* 2019, 2019 (37), 4031–4039.
35. Cho J; Furutachi H; Fujinami S; Suzuki M A Bis(μ -alkylperoxo)nickel(II) Complex as a Reaction Intermediate for the Oxidation of the Methyl Groups of the Me₂-tpa Ligand to Carboxylate and Alkoxide Ligands. *Angew. Chem. Int. Ed* 2004, 43 (25), 3300–3303.
36. McCusker JK; Rheingold AL; Hendrickson DN Variable-Temperature Studies of Laser-Initiated $^5\text{T}_2 \rightarrow ^1\text{A}_1$ Intersystem Crossing in Spin-Crossover Complexes: Empirical Correlations between Activation Parameters and Ligand Structure in a Series of Polypyridyl Ferrous Complexes. *Inorg. Chem* 1996, 35 (7), 2100–2112.
37. Marchivie M; Guionneau P; Létard J-F; Chasseau D Photo-induced spin-transition: the role of the iron(II) environment distortion. *Acta Crystallogr. Sect. B: Struct. Sci* 2005, 61 (1), 25–28.
38. Bunker PRJ, *Per Molecular Symmetry and Spectroscopy*. NRC Research Press, Ottawa 1998.
39. Schmiedekamp AM; Ryan MD; Deeth RJ Six-Coordinate Co^{2+} with H_2O and NH_3 Ligands: Which Spin State Is More Stable? *Inorg. Chem* 2002, 41 (22), 5733–5743. [PubMed: 12401078]
40. Rossi AR; Hoffmann R Transition metal pentacoordination. *Inorg. Chem* 1975, 14 (2), 365–374.

41. Bertini I; Luchinat C High spin cobalt(II) as a probe for the investigation of metalloproteins. *Adv. Inorg. Biochem* 1984, 6, 71–111. [PubMed: 6442958]
42. Tubbs KJ; Szajna E; Bennett B; Halfen JA; Watkins RW; Arif AM; Berreau LM Mononuclear nitrogen/sulfur-ligated cobalt(ii) methoxide complexes: Structural, EPR, paramagnetic ¹H NMR, and electrochemical investigations. *Dalton Trans.* 2004, (16), 2398. [PubMed: 15303148]
43. Jolly WL *The synthesis and characterization of inorganic compounds*. Prentice Hall: Hoboken, 1970.
44. Barefield EK; Busch DH; Nelson SM Iron, cobalt, and nickel complexes having anomalous magnetic moments. *Q. Rev. Chem. Soc* 1968, 22 (4), 457.
45. Lewis BNFJ *In Progress in Inorganic Chemistry*; 1 ed.; Cotton FA, Ed.; Wiley: Hoboken, 1964; Chapter 2, Vol. 6, pp 37–239.
46. Banci L; Bencini A; Benelli C; Gatteschi D; Zanchini C *In Structures versus Special Properties*; 1 ed.; Springer Berlin, 1982; Vol. 52, pp 37–86.
47. Farrukh MA *Advanced Aspects of Spectroscopy*. IntechOpen: London, 2012.
48. Makowska-Grzyska MM; Szajna E; Shipley C; Arif AM; Mitchell MH; Halfen JA; Berreau LM First Row Divalent Transition Metal Complexes of Aryl-Appended Tris((pyridyl)methyl)amine Ligands: Syntheses, Structures, Electrochemistry, and Hydroxamate Binding Properties. *Inorg. Chem* 2003, 42 (23), 7472–7488. [PubMed: 14606843]
49. Basu Baul TS; Nongsiej K; Rocha BGM; Guedes da Silva MFC Cobalt(II) complexes with pyridine and 5-[(E)-2-(aryl)-1-diazenyl]-quinolin-8-olates: synthesis, electrochemistry and X-ray structural characterization. *J. Coord. Chem* 2018, 71 (16–18), 2856–2874.

Synopsis

Picolinic acid, several picolinic acid metal binding isosteres (MBIs), and 2,2'-bipyridine were examined using a bioinorganic model system of metalloenzyme inhibition [M(TPA)(MBI)] ($M = \text{Ni}^{2+}$ and Co^{2+} , TPA = tris(2-pyridylmethyl)amine). These complexes were characterized using synthetic, structural, and spectroscopic methods. [(Tp^{Ph,Me})Co(MBI)] (Tp^{Ph,Me} = hydrotris(3,5-phenylmethylpyrazolyl)borate) was used as another model system and the limitations and attributes of the two model systems are discussed.

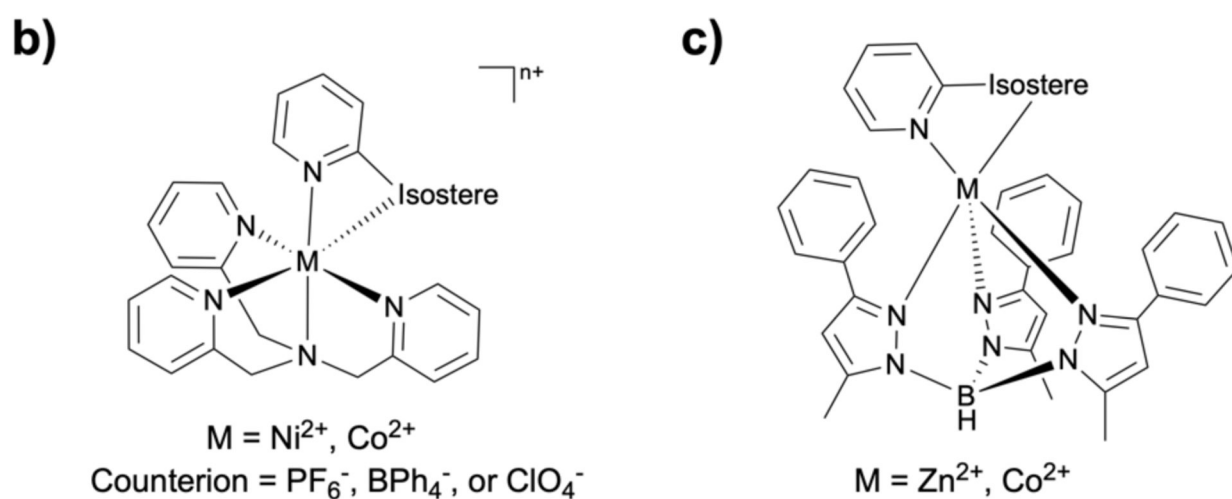
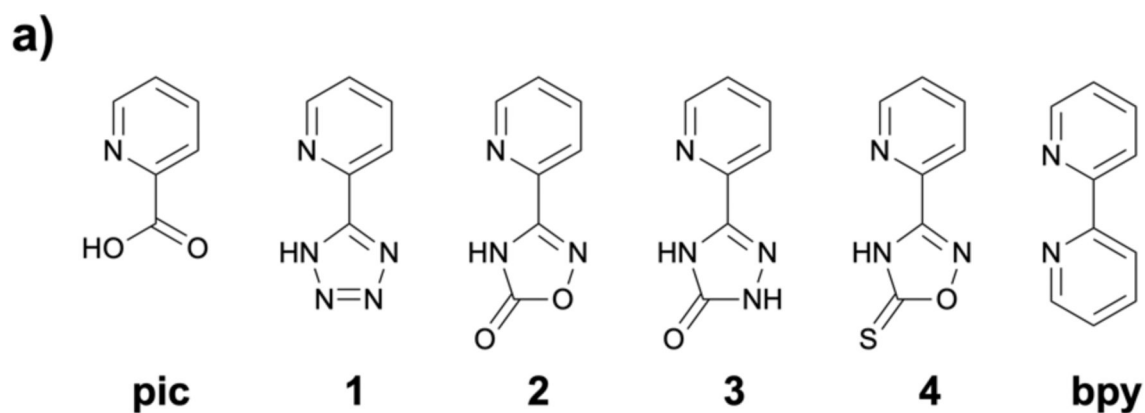


Figure 1.

a) Picolinic acid (pic), MBIs of picolinic acid, and 2,2'-bipyridine (bpy). b) Chemical structure of the [M(TPA)(MBI)]⁺ model system (TPA = tris(2-pyridylmethyl)amine). c) Chemical structure of the [(Tp^{Ph,Me})Zn(MBI)] model system (Tp^{Ph,Me} = hydrotris(5,3-methylphenylpyrazolyl)borate).

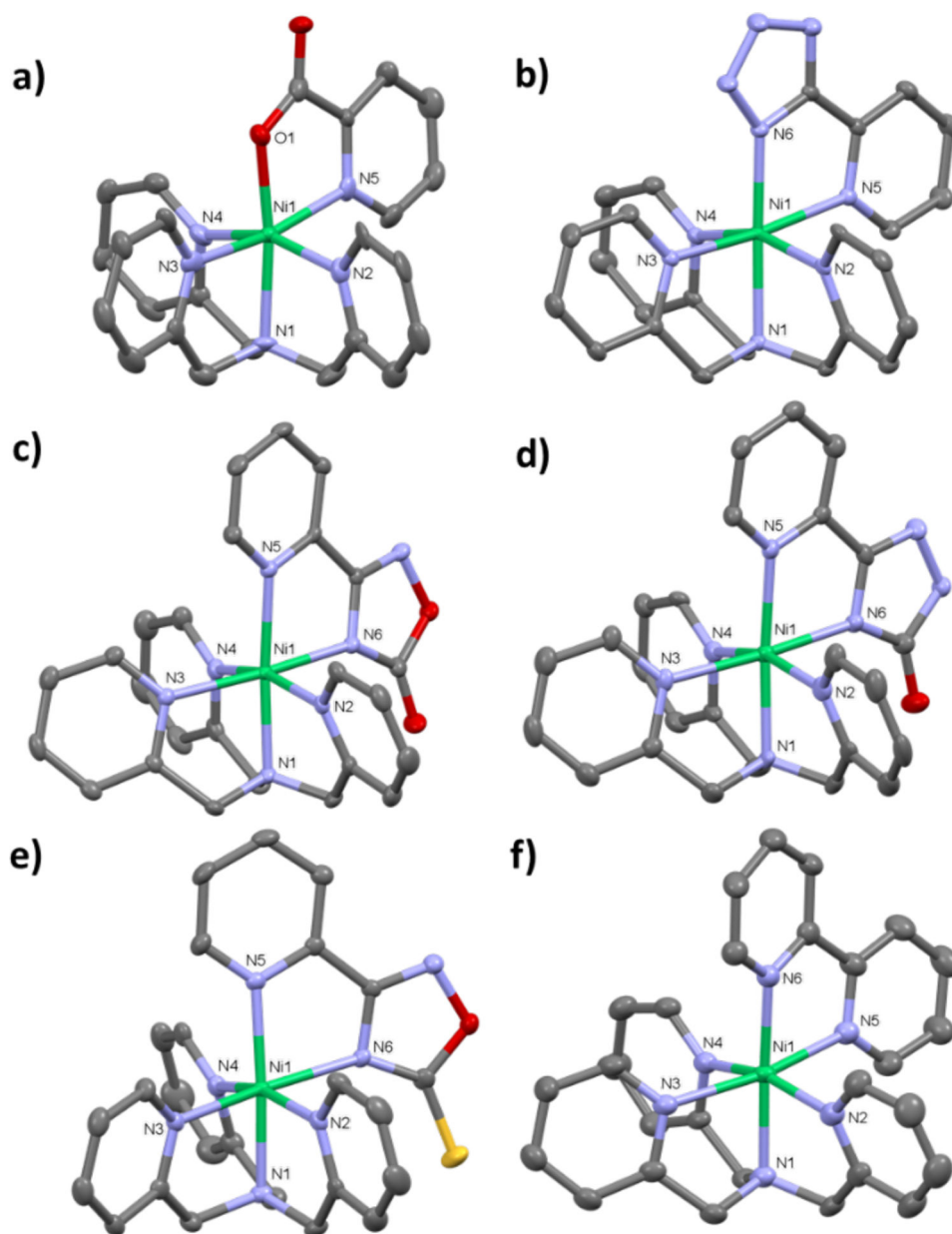


Figure 2. Crystal structures of [Ni(TPA)(L)] complexes (ORTEP, 50% probability ellipsoids). a) [Ni(TPA)(pic)]⁺, b) [Ni(TPA)(1)]⁺, c) [Ni(TPA)(2)]⁺, d) [Ni(TPA)(3)]⁺, e) [Ni(TPA)(4)]⁺, f) [Ni(TPA)(bpy)]²⁺. Solvent molecules, counter ions, and hydrogen atoms have been omitted for clarity. Donor atoms are alphanumerically labelled. Color scheme: carbon = gray, oxygen = red, nitrogen = blue, nickel = green, and sulfur = yellow.

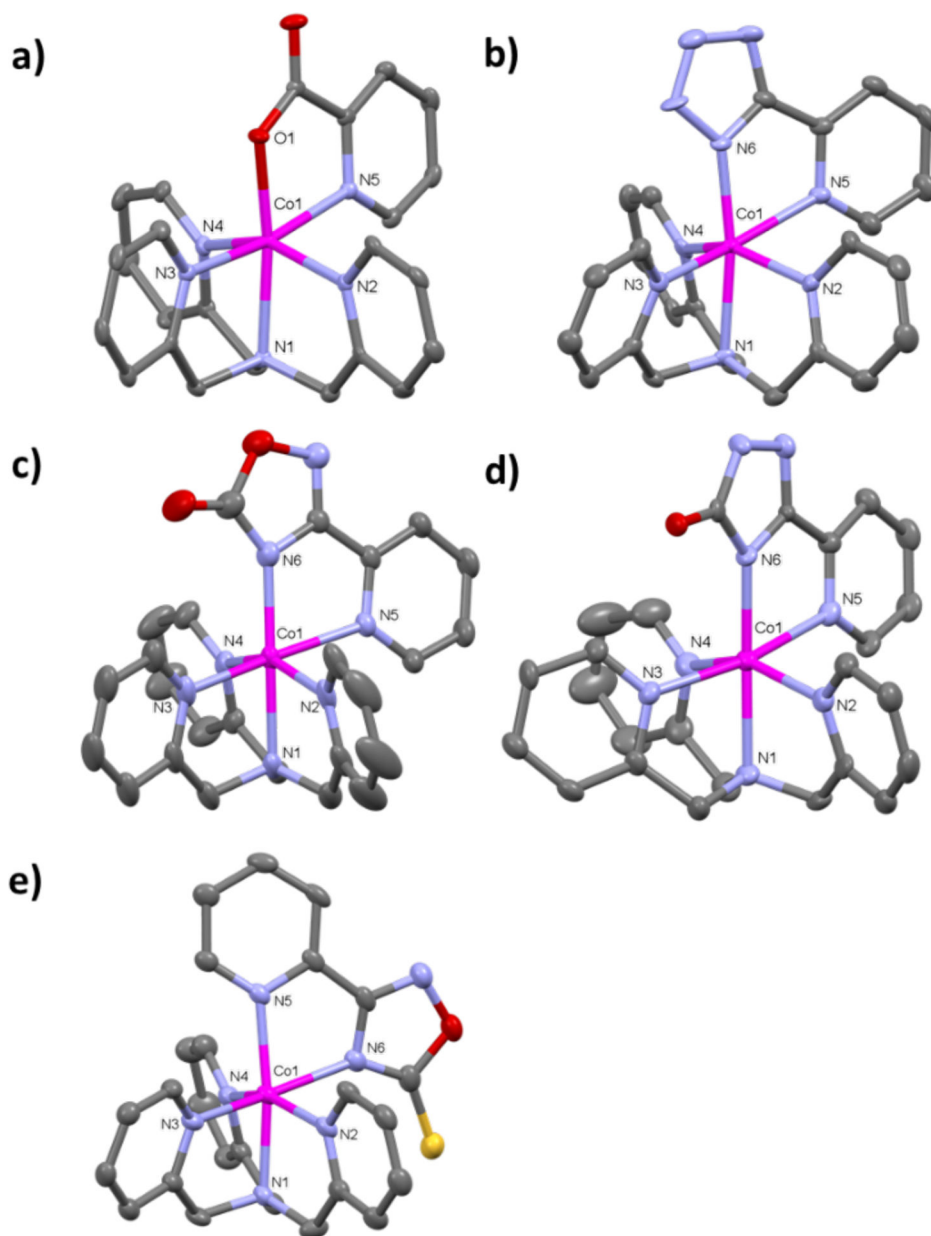


Figure 3. Crystal structures of $[\text{Co}(\text{TPA})(\text{L})]$ complexes (ORTEP, 50% probability ellipsoids). a) $[\text{Co}(\text{TPA})(\text{pic})]^+$, b) $[\text{Co}(\text{TPA})(\mathbf{1})]^+$, c) $[\text{Co}(\text{TPA})(\mathbf{2})]^+$, d) $[\text{Co}(\text{TPA})(\mathbf{3})]^+$, e) $[\text{Co}(\text{TPA})(\mathbf{4})]^+$. Solvent molecules, counter ions, and hydrogen atoms have been omitted for clarity. Donor atoms are alphanumerically labelled. Color scheme: carbon = gray, oxygen = red, nitrogen = blue, cobalt = pink, and sulfur = yellow.

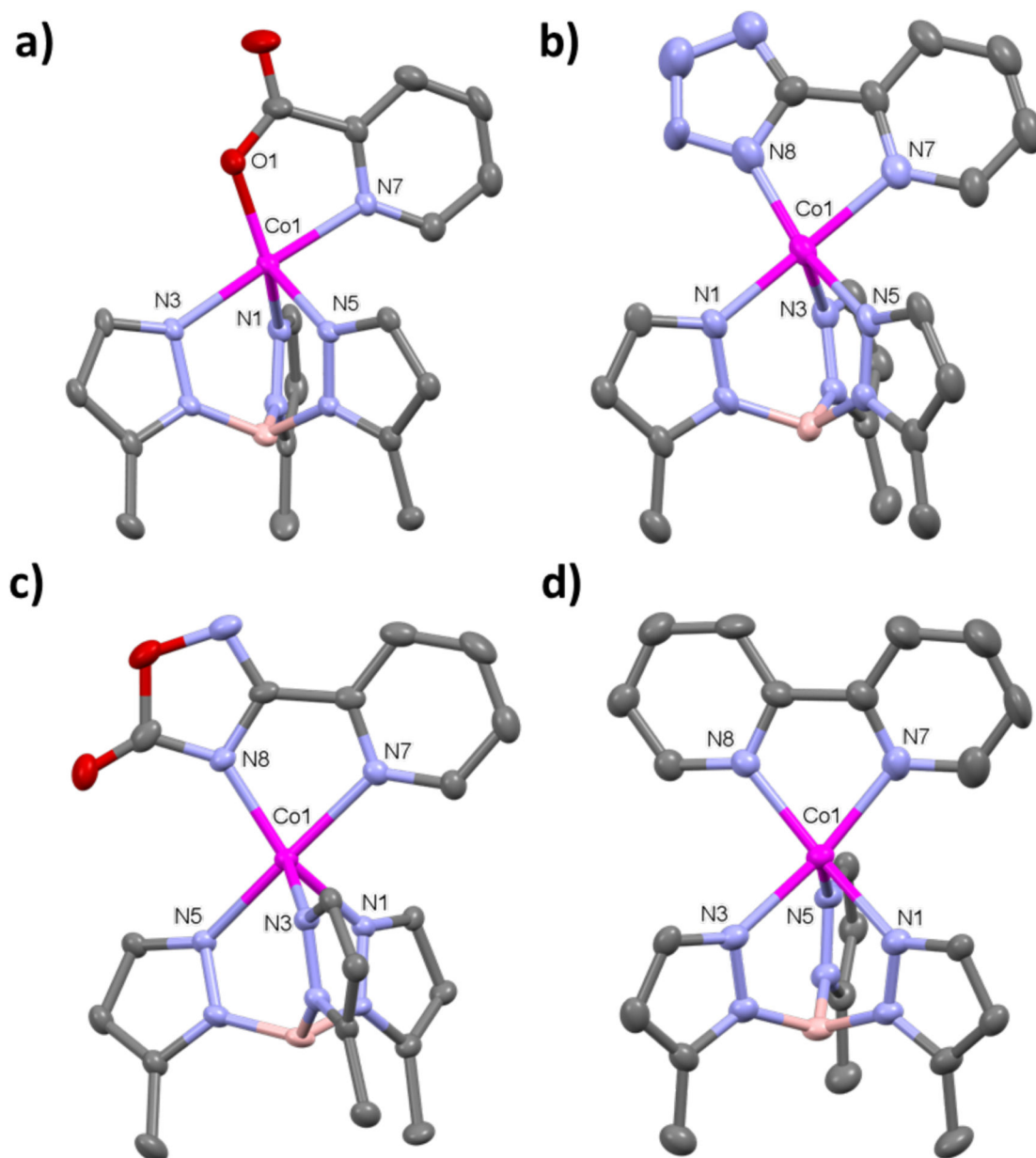


Figure 4. Crystal structures of $[(\text{Tp}^{\text{Ph,Me}})\text{Co}(\text{L})]$ complexes (ORTEP, 50% probability ellipsoids). a) $[(\text{Tp}^{\text{Ph,Me}})\text{Co}(\text{pic})]$, b) $[(\text{Tp}^{\text{Ph,Me}})\text{Co}(\text{1})]$, c) $[(\text{Tp}^{\text{Ph,Me}})\text{Co}(\text{2})]$, d) $[(\text{Tp}^{\text{Ph,Me}})\text{Co}(\text{bpy})]$. Phenyl groups of $\text{Tp}^{\text{Ph,Me}}$ have been omitted for clarity. Donor atoms are alphanumerically labelled. Color scheme: carbon = gray, oxygen = red, nitrogen = blue, cobalt = pink, and boron = pink.

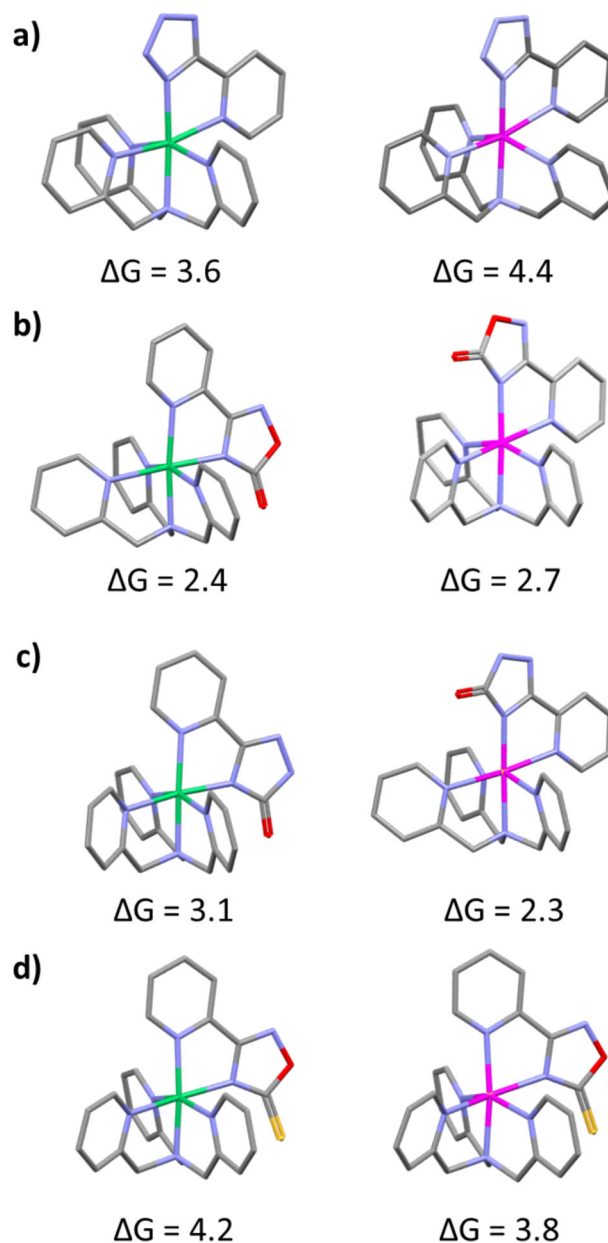


Figure 5. Computationally optimized structures and relative free Gibbs energy differences of the binding orientation isomers of the MBI **1 - 4** coordinated to Ni(II) (*left*) or Co(II) (*right*) TPA complexes at the wB97x-D/LanL2DZ level of theory. a) [Ni(TPA)(**1**)]⁺ and [Co(TPA)(**1**)]⁺, b) [Ni(TPA)(**2**)]⁺ and [Co(TPA)(**2**)]⁺, c) [Ni(TPA)(**3**)]⁺ and [Co(TPA)(**3**)]⁺, d) [Ni(TPA)(**4**)]⁺ and [Co(TPA)(**4**)]⁺. Color scheme: carbon = gray, oxygen = red, nitrogen = blue, nickel = green, cobalt = pink, and sulfur = yellow.

Table 1.

Selected bond lengths and angles for [Ni(TPA)(L)]. Structures with more than one complex in the asymmetric unit are marked with an asterisk.

Ligand	Ni-N5 (Å)	Ni-O1/N6 (Å)	Bite angle (°)	Sigma, Theta (Σ , Θ) (°)
Pic*	2.126(9)	1.984(8)	80.1(3)	89, 287
	2.129(9)	2.003(8)	80.0(3)	89, 294
1	2.231(4)	2.039(3)	77.99(15)	83, 258
2	2.111(2)	2.110(2)	79.70(9)	98, 257
3*	2.128(4)	2.123(4)	79.31(14)	100, 274
	2.116(4)	2.114(4)	79.52(14)	94, 240
	2.093(4)	2.104(4)	80.14(14)	99, 250
4	2.072(3)	2.155(3)	79.59(9)	101, 288
bpy	2.148(3)	2.054(3)	78.51(12)	104, 302

Table 2.

Selected bond lengths and angles for [Co(TPA)(L)]. Structures with more than one complex in the asymmetric unit are marked with an asterisks.

Ligand	Co-N5 (Å)	Co-O1/N6 (Å)	Bite angle (°)	Sigma, Theta (, Θ) (°)
pic	2.178(3)	2.012(2)	78.87(9)	113, 360
1*	2.317(5)	2.058(5)	75.2(2)	141, 490
	2.307(6)	2.058(6)	75.5(2)	132, 424
	2.320(6)	2.057(6)	75.3(2)	129, 416
	2.357(6)	2.062(5)	74.5(2)	142, 458
2	2.2743(18)	2.073(2)	77.22(7)	111, 302
3	2.267(3)	2.060(3)	76.94(12)	130, 386
4	2.130(3)	2.181(3)	77.48(11)	121, 401
	2.204(3)	2.161(3)	76.74(11)	122, 359

Table 3.Selected bond lengths and angles for [(Tp^{Ph,Me})Co(L)].

Ligand	Co-N7 (Å)	Co-O1/N8 (Å)	Bite angle (°)	Tau, τ (°)
pic	2.135(3)	1.965(2)	79.97(9)	0.71
1	2.145(4)	1.963(4)	78.48(17)	0.32
2	2.167(4)	2.023(4)	78.17(16)	0.41
bpy	2.080(3)	2.069(3)	78.09(13)	0.01

Table 4.

UV-visible and magnetic moment data for TPA complexes.

Ligand	[Ni(TPA)(L)] ⁿ⁺		[Co(TPA)(L)] ⁿ⁺	
	μ_{eff} , B.M.	λ_{max} , nm (ϵ , M ⁻¹ cm ⁻¹)	μ_{eff} , B.M.	λ_{max} , nm (ϵ , M ⁻¹ cm ⁻¹)
pic	3.16	531 (21)	4.60	493 (103)
1	3.12	534 (23)	4.76	485 (117)
2	3.33	548 (21)	4.56	486 (64)
3	3.32	552 (19)	4.74	484 (88)
4	3.34	555 (16)	4.62	483 (76)
bpy	3.09	576 (21)	-	-

Table 5.

UV-visible and magnetic moment data for Tp complexes.

[(Tp ^{Ph,Me})Co(L)] ⁿ⁺		
Ligand	μ_{eff} , B.M.	λ_{max} , nm (e, M ⁻¹ cm ⁻¹)
pic	4.84	452 (41), 538 (49), 561 (51)
1	4.84	456 (37), 540 (49), 563 (47)
2	4.85	448 (47), 542 (44), 562 (42)
bpy	4.66	417 (333), 520 (76), 676 (34)